Structural Characterization of Tau Fibrils with N410M Modification: Comparative Analysis of CryoSPARC and RELION in Neurodegenerative Disease Research

by

Daya Stevens

Department of Psychology and Neuroscience

University of Colorado Boulder

Boulder, Colorado 80309

Defense Date: Tuesday, 8 April 2025

Honors Thesis Advisor: Michael Stowell

Defense Committee:

Michael Stowell, Department of Molecular, Cellular, and Developmental Biology, Honors Thesis Advisor

David Allen, Department of Psychology and Neuroscience, Honors Council Representative

Jennifer Stratford, Department of Psychology and Neuroscience, Outside Reader

Abstract

Neurodegenerative diseases affect approximately 15% of the global population, yet their underlying causes largely remain unknown. A common feature of these disorders, including Alzheimer's Disease (AD), is the accumulation of misfolded proteins in the brain. One protein that readily forms these aggregates is Tau. Tau is associated with the assembly and stabilization of microtubules, which maintain the structure and function of neurons. Tau exhibits noticeable structural variance due to factors such as fibrillization and post-translational modifications, including glycosylation. Glycosylation, specifically N-glycosylation at the N410 position on Tau, has been shown to be altered in AD brain and not in healthy brain. Our lab has investigated synthetic Tau, N410M, using cryo-electron microscopy (cryo-EM) to determine its structural characteristics. This study provides a comparative analysis of cryo-EM software programs, CryoSPARC and RELION, in obtaining helical reconstructions of N410M, offering insights into the advantages and limitations of each for structural determination.

Introduction

Dementia is the seventh leading cause of death, and it is estimated that more than 55 million people have dementia worldwide (World Health Organization, 2024). That number is expected to double every 20 years, reaching 78 million people in 2030 and 139 million in 2050 (Alzheimer's Disease International, n.d.). Alzheimer's disease is the leading cause of dementia, accounting for 60-70% of cases. Despite increasing prevalence, there is no cure for dementia (World Health Organization, 2024), highlighting the urgency of understanding the molecular mechanisms underlying these pathologies.

Tau is a crucial microtubule-associated protein (MAP), making up over 80% of neuronal MAPs. It plays a key role in stabilizing microtubules, which are essential for maintaining neuronal structure and facilitating intracellular transport (Kellogg et al., 2018). Under normal physiological conditions, Tau is hypothesized to promote microtubule stability and ensure proper cellular function (Barbier et al., 2019). Tau undergoes post-translational modifications (PTMs) such as phosphorylation, acetylation, and glycosylation that affect Tau's structure and function. In diseased brain, Tau undergoes abnormal PTMs, impairing its ability to bind to microtubules (MTs) (Guo et al., 2017). As a result, Tau dissociates from MTs and aggregates into pathological fibrils known as neurofibrillary tangles (NFTs) (Oakley et al., 2020). A hallmark of Alzheimer's disease and other tauopathies, such as frontotemporal dementia and chronic traumatic encephalopathy, is the accumulation of misfolded Tau in the core of NFTs (Guo et al., 2017). Certain PTMs stabilize components of NFTs and promote Tau's tendency to misfold and aggregate, contributing to tauopathies (Oakley et al., 2020). Notably, N-glycosylation—a specific type of PTM—at position 410 on Tau is altered in AD brain but not in healthy brain (Zhang et al., 2024).

Although Tau aggregation is a prominent feature of tauopathies, the structural determinants that drive these abnormal fibril formations remain unclear. Cryo-electron microscopy (cryo-EM) studies have shown that different tauopathies exhibit distinct fibrillar polymorphs, suggesting that structural differences may underlie disease-specific pathology (Oakley et al., 2020). Recent research has shown that N410M, a form of Tau with a mannose addition at amino acid 410, is found in AD brain but not in healthy brain (Zhang et al., 2024). This emphasizes the importance of exploring its structural determination.

By synthesizing N410M Tau and analyzing its fibrillar structure using cryo-EM, we aim to compare how this modification affects the structure of Tau fibrils in two leading helical reconstruction software platforms, CryoSPARC and RELION. CryoSPARC, preferred for its user-friendly interface and speed, is the program I selected to obtain a high-resolution reconstruction of N410M. However, RELION remains widely used due to its long-standing reputation, extensive validation in the field, and adoption by many experienced researchers who were trained on it. It is also free and semi-open source, making it accessible to a broader scientific community (MRC Laboratory of Molecular Biology, n.d.). I aim to compare the results from the two separate pipelines used by RELION and CryoSPARC use on the same dataset to determine whether CryoSPARC's ease of use yields results comparable to RELION's well-established helical reconstruction software.

This comparative analysis of CryoSPARC and RELION for the structural determination of Tau fibrils with post-translational modification N410M highlights the importance of exploring alternative tools, such as CryoSPARC, due to RELION's complex user interface, aiming to improve accessibility, scalability, and user-friendliness in cryo-EM, ultimately advancing research on amyloid fibrils implicated in neurodegenerative diseases.

Background

Tau Structure and Function

General tau biology. Tau is a microtubule-associated protein that promotes microtubular assembly and stability in axons of neurons. Human Tau is expressed primarily in neurons, with lower levels found in oligodendrocytes and astrocytes. Tau is mainly located in axons, with lower amounts in dendrites. Current evidence suggests Tau may modulate the formation and trafficking of stress granules, which is significant for both the neuronal stress response and the development of various neurodegenerative diseases (Guo et al., 2017).

Tau isoforms and domains. Human Tau is encoded by the *MAPT* gene located on chromosome 17 and is expressed in the central nervous system (CNS) as a family of six isoforms (Oakley et al., 2020). The structure of Tau is proposed to be important for its normal functioning as its domains form a flexible, low-secondary structure protein that allows Tau to bind and stabilize microtubules. The C-terminal region is common to all six human CNS Tau isoforms. One published structure of healthy Tau shows the C terminus folds over the microtubule binding domain and the N terminus folds back over the C terminus, bringing the termini into tight proximity in a paperclip-like structure. This spatial closeness between termini and overall structure of Tau can be loosened upon Tau binding to microtubules as well as phosphorylation (Guo et al., 2017). Tau is classified into four domains, the N-terminal domain (NTD), proline-rich domain (PRD), microtubule-binding domain (MTBD), and the C-terminal domain (CTD). The N-terminal domain is acidic and contains two alternatively spliced inserts, so tau can exist in different isoforms depending on their inclusion. The proline-rich domain (PRD) contains proline residues and connects the N-terminal to the microtubule-binding domain. The microtubule-binding domain (MTBD) is a part of the C-terminal domain and contains four repeats, separated

by regions that contribute to Tau's ability to bind and stabilize microtubules. The second and third repeated motifs of the MTBD tend to form beta-sheets (Guo et al., 2017), which are commonly associated with protein aggregation in tauopathies (Li et al., 2023). The C-terminal domain regulates tau's ability to aggregate and interact with other proteins, as it binds to microtubules and promotes their assembly making it the most flexible part of the protein (Mietelska-Porowska et al., 2014).

For this study, Tau 2N4R, the full-length Tau isoform, was used:

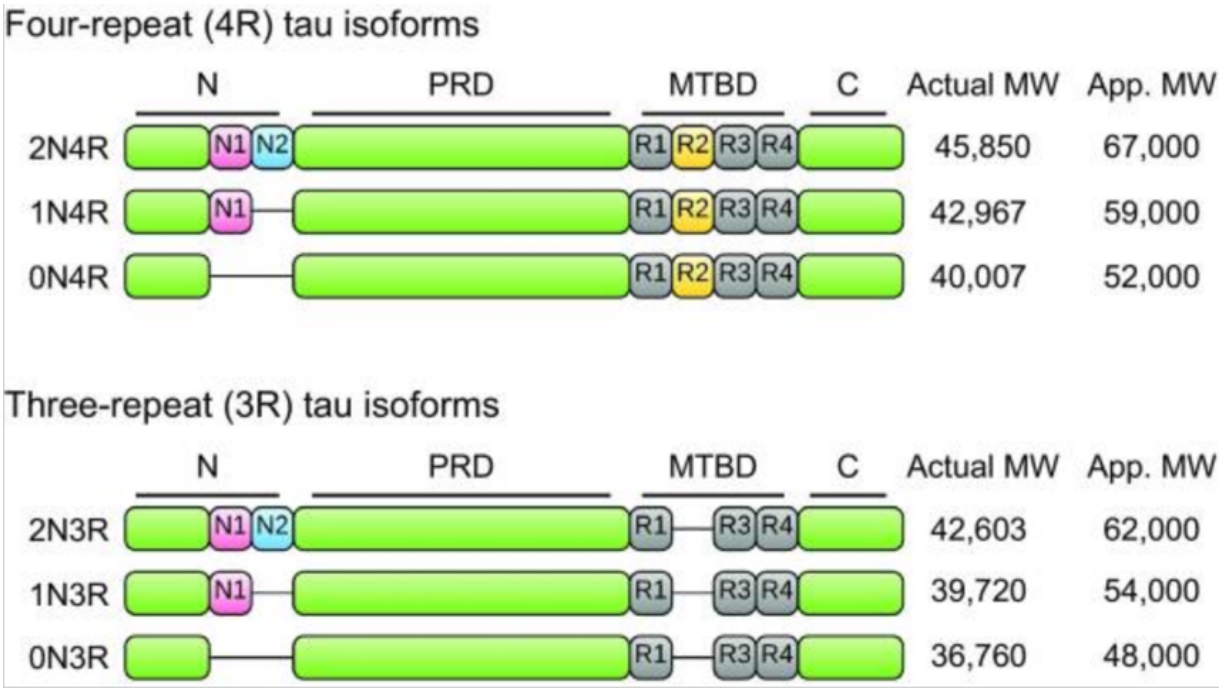

Fig. 1 Six human isoforms of Tau. N-terminal regions of Tau (0N, 1N, or 2N) give rise to the individual isoform and C-terminal regions are common to all six isoforms (Guo et al., 2017).

Normal role of Tau. The primary function of Tau is to stabilize microtubules by reducing the dissociation of tubulin at both ends of the microtubule. This results in an increased growth rate, and a decrease in depolymerization and catastrophe frequency. Tau acts as one of

two of the major microtubule associated proteins (MAPs) in the CNS, the other one being MAP2 (Barbier et al., 2019).

Tau misfolding and aggregation. Under pathological conditions, the abnormal assembly of Tau into aggregates is associated with synaptic dysfunction and neuronal cell death in various neurodegenerative disorders, collectively referred to as tauopathies (Guo et al., 2017). Alzheimer's disease (AD) is characterized by the presence of extracellular amyloid plaques, composed of β-amyloid peptide (Aβ) and intracellular neurofibrillary tangles (NFTs), composed of Tau. NFTs are composed of paired helical filaments (PHFs) and straight filaments (SFs), both of which are formed by Tau, with Tau being the major structural component of the PHF core. In AD, the majority, 90%, of Tau aggregates exist within the PHFs (Oakley et al., 2020).

Post-translational Modifications

Types of PTMs. Tau is subject to a wide range of post-translational modifications (PTMs), including phosphorylation, glycosylation, acetylation, isomerization, glycation, and nitration. PTMs, such as phosphorylation and glycosylation, stabilize PHFs (Oakley et al., 2020). Phosphorylation is the addition of phosphate groups at specific phosphorylation sites along the protein sequence, and hyperphosphorylation of Tau is hypothesized to be the primary contributing factor to fibril formation and neurofibrillary tangles in tauopathies (Brion et al., 2001). Glycosylation is the attachment of oligosaccharides to amino acids in the protein, involving the addition of carbohydrate molecules. There are two types of glycosylations: N-glycosylation and O-glycosylation (Mietelska-Porowska et al., 2014). PHFs are glycosylated at residues at which normal Tau proteins from healthy brain are not. Isolated from AD brains, PHF-

Tau and hyperphosphorylated Tau had a higher abundance of truncated glycans, incompletely processed sugar chains, and high mannose-type sugar chains (Sato et al., 2001).

Tau N410M

Biology. Semi-synthetic N410M Tau protein was created using a combination of expressed protein ligation (for amino acid residues 2-290) and native chemical ligation for the remainder of the protein (amino acid residues 291-441). This combination of procedures allowed for high protein yield, as well as allowing us to add a mannose PTM to a specific N-linked glycosylation site at asparagine 410 (N410) (Powell et al., 2025).

N410M in diseased brains. N410 was selected as the glycosylation site as previous studies have showed that this specific site, N410, was N-glycosylated by a high-mannose-type glycan *in vivo* in AD brain and not in healthy brain. The ability to create semi-synthetic N410M Tau with the same mannose addition as diseased brain can provide us with more insight to the nature of PTMs in regards to diseased-Tau structure, as there is strong support for the involvement of altered N-glycan modifications of the AD-related proteins (Zhang et al., 2024).

Native chemical ligation. Native chemical ligation (NCL) is a powerful technique used in protein synthesis that allows for precise chemical assembly of proteins from smaller peptide fragments. It is particularly useful for incorporating PTMs, like glycosylation, at specific sites (Hackeng et al., 1999). Recombinant Tau expression poses significantly more challenges in specific glycosylation. Expressing the entirety of the Tau protein recombinantly in E. coli, for example, cannot add glycosylation since the bacteria lack the necessary enzymes to do so. Mammalian expression systems can glycosylate proteins, but the modification may not be uniform between individual protein molecules and may occur at multiple unintended sites

(Wilson et al., 1994). Synthesis of a region of interest NCL allows for site-specific control to test for disease-related modifications.

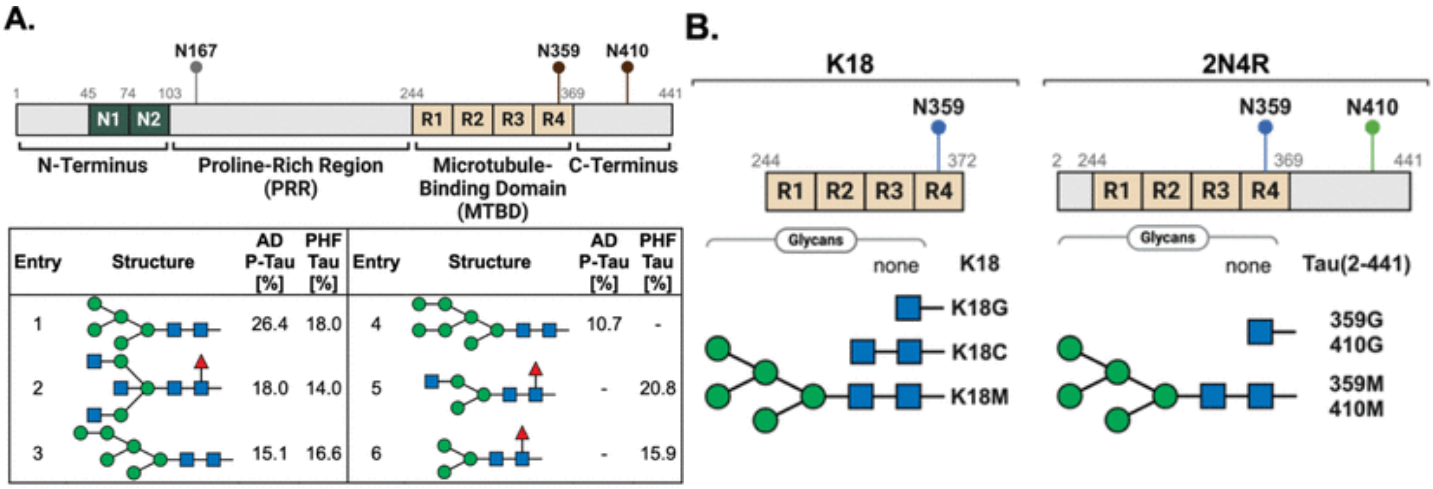

Fig. 2 (A) The domain organization of 2N4R Tau used, highlighting the positions of N-linked glycans and the glycan structure observed in AD patients. (B, right side) The N-glycosylated Tau construct (N410M) used in this study (Powell et al., 2025).

Importance of Structural Determination

Understanding fibril structure & variability. Previous studies using Cryo-EM have revealed that Tau filaments consist of two identical protofilaments forming a combined cross-β/β-helix structure. Research has demonstrated that Tau filaments exhibit polymorphism, meaning the protein adopts different configurations depending on conditions such as PTMs. Structural differences are associated with corresponding tauopathies which highlights the role of structural variation in disease manifestation (WP Fitzpatrick et al., 2017).

Aggregation mechanism insight. High-resolution imaging has provided detailed views of the assembly of Tau fibrils, which allow for more information on its aggregation. Understanding the mechanisms behind Tau aggregation is crucial in developing therapeutic

strategies for Tau-related diseases such as AD (Duan et al., 2024). With recent studies identifying specific regions within Tau fibrils where certain PTMs, such as glycosylation, occur, imaging can show how these modifications influence Tau fibril stability and contribution to disease progression (Zhang et al., 2019).

Cryo-EM Advantages for Structural Determination of Fibrils

Cryo-electron microscopy provides several distinct advantages for the imaging of Tau fibrils. Cryo-EM can achieve near atomic resolutions, allowing for detailed structural analysis. One publication presented a cryo-EM structure of full-length Tau fibrils induced by RNA from mouse liver, using human wild-type Tau expressed in E. Coli, at 3.4 Å resolution. The structure revealed a 36-residue C-terminal fibril core bound to RNA (Abskharon et al., 2021). Cryo-EM techniques also preserve samples in a near-native state by flash-freezing them, maintaining their natural conformations without the need for crystallization like X-ray crystallography (Ghosh et al., 2024). Cryo-EM can also effectively analyze heterogenous samples, allowing for the capturing of multiple conformations of the same protein within a single dataset (Shuimu BioSciences, n.d.). Research has used cryo-EM to reveal ultrastructural polymorphs of PHFs and SFs in amyloid filaments (Fitzpatrick et al., 2017).

About RELION

RELION (*Regularized Likelihood Optimization*) was first released in 2012 and is primarily a command-line-based program with a graphical user interface (GUI) designed for the refinement of macromolecular structures using single-particle analysis (SPA) and helical reconstruction (RELION, n.d.). RELION employs a Bayesian statistical approach to derive model parameters

directly from the data for improved accuracy (Scheres, 2012). In October 2019, RELION introduced version 3.1, allowing for helical reconstruction to be conducted within the program without the need for external tools (Scheres & He, 2017). Version 3.1 and up include the relion_helix_inimodel2d program and adds parameters in other jobs of the reconstruction pipeline optimized for helical filaments. The relion_helix_inimodel2d program generates a 2D map to use as an initial 3D reference for a helical structure by aligning 2D class averages to form a continuous density map spanning an entire cross-over region— critical for amyloid fibril analysis (RELION, n.d.). The addition of helix-specific parameters to the particle Autopicking step also allows for a more precise selection of helices. RELION's Expectation-Maximization (EM) algorithm is recommended for 2D classification of helices, following these steps:

- The E-step (Expectation) computes probabilities for particle orientations.
- The M-step (Maximization) refines particle alignment and updates the 2D structure model.

About CryoSPARC

CryoSPARC (*Cryo-EM Single Particle Ab-Initio Reconstruction and Classification*) was first released in 2017 and is a high-performance computing (HPC) software designed for complete processing of single-particle cryo-EM data. CryoSPARC is widely used for obtaining high-resolution structures of membrane proteins, viruses, or protein complexes (Structura Biotechnology Inc., n.d.). A key feature of CryoSPARC is its ability to automatically generate an ab-initio 3D reconstruction using a stochastic gradient descent (SGD) optimization approach, eliminating the need for user-provided initial models. Additionally, CryoSPARC employs a modified Expectation-Maximization (EM) algorithm combined with variational Bayesian

inference for enhanced particle alignment and classification. Its 2D classification algorithm clusters particles into classes using a maximum-likelihood approach, similar to RELION, but with enhanced speed on larger datasets due to better GPU acceleration. CryoSPARC references Punjani et al. (2017) to provide a comprehensive pipeline that covers preprocessing, 2D classification, Ab-initio reconstruction, Refinement (Structura Biotechnology Inc., n.d.).

While CryoSPARC is known for its user-friendly interface and intuitive workflow, it lacks specialized tools for the refinement of amyloid fibrils, unlike RELION (Structura Biotechnology Inc., n.d.).

Literature Review

Helical reconstruction studies on Tau fibrils have predominantly utilized RELION, with a considerable body of literature documenting its application and efficacy in this domain. Recent major findings in cryo-EM structures of Tau filaments were found in Down syndrome (Fernandez et al., 2024) and in Alzheimer's disease (WP Fitzpatrick et al., 2017) brain using RELION's helical reconstruction pipeline to determine the structures. In contrast, there is limited documentation addressing the use of CryoSPARC for helical reconstruction, particularly with respect to Tau fibrils. CryoSPARC (Structura Biotechnology Inc., n.d.) as well as reviewers (CryoSPARC Discussion Forum, n.d.) have also acknowledged difficulties with processing data of amyloid fibrils. This gap in the existing research highlights the importance of further exploration of CryoSPARC's potential helical reconstruction. Additionally, this research will provide a non-industry and unbiased perspective on the relative quality, user-friendliness, and potential advantages of CryoSPARC when applied to helical structures in comparison to RELION.

This publication (Scheres, 2020) offers insight into the methodology of helical reconstruction of amyloid filaments, particularly Tau filaments, using RELION-3.1. Scheres acknowledges the increasing importance of cryo-EM for studying the atomic-level structure of amyloid filaments, such as those involved in neurodegenerative diseases. Scheres discusses the early techniques that applied the single-particle approach to helical reconstruction, which were initially performed in real space (Scheres, 2020). *Real space* is a mathematical concept that represents the direct physical space where objects or particles are located, described using spatial calculations (Nishikawa, 2003). In 2000, the *iterative helical real-space reconstruction* (IHRSR)

algorithm was developed and improved upon earlier techniques by refining the structures in real space iteratively or making small corrections to the reconstruction over several cycles (Egelman, 2000). This allowed for a broader application of helical reconstruction in cryo-EM. In 2017, a similar approach was incorporated into the *empirical Bayesian framework* of RELION, which operates in a mathematical space called Fourier space. This method uses statistical techniques to predict how much individual parts of a helical structure can deviate from each other. The first determination of cryo-EM structures of amyloid filaments at sufficient resolution for de novo atomic model building was achieved for the paired helical filaments (PHFs) formed by Tau protein in Alzheimer's disease, while the structure of straight filaments (SFs) remained elusive (Scheres, 2020). Since then, RELION has been used to solve several cryo-EM structures of amyloids. RELION has been the primary tool for amyloid and Tau fibril studies due to its well-developed helical processing pipeline, but challenges can arise from the structural variability of amyloids. Scheres aims to guide RELION-users through amyloid helical reconstruction determination by discussing amyloid-specific aspects, illustrating the issues with local optima in refinement, and introducing new methods to obtain 3D initial models from reference-free 2D class averages (Scheres, 2020). The authors developed a new method, using Fourier space, for generating initial 3D models from 2D class averages in RELION-3.1 to address the IHRSR algorithm's tendency to converge at local minima. This allows deviations from the perfect helical symmetry to be incorporated into the model, which improves the refinement process. In applying this new method to Tau filaments, specifically from AD brain, they were able to significantly improve the resolution of structures, which allowed for the construction of high-resolution models of PHFs that Tau forms. The development of this new method to generate initial 3D models from 2D class averages in RELION-3.1 is effective in solving helical reconstructions and

opens up possibilities for solving more complex amyloid structures at high resolution, which will aid in furthering the study of neurodegenerative disease and protein misfolding.

This publication (Lövestam & Scheres, 2022) describes a new filament picking algorithm in RELION using Topaz and outlines image processing strategies to use that allow for the structural determination of amyloids in just a few days. Their approach modifies the Topaz program for filament picking to enhance the identification of amyloid filaments within cryo-EM data. The Topaz pipeline consists of three main steps: preprocessing micrographs with RELION's wrapper, training a convolutional neural network on labeled and unlabeled data, and using a sliding window to classify particle and extract coordinates by non-maximum suppression. The authors refined the image processing steps in RELION, integrating multiple techniques for faster, higher-resolution structure determination. The study also addresses the issue of local minima in helical refinement, where the optimization process converges on suboptimal solutions rather than the true global minimum. In their discussion, they highlight how getting stuck in local minima continues to be the largest pitfall of amyloid structure determination, leading to inaccuracies in filament reconstruction and model building.

Despite RELION's dominance, CryoSPARC is gaining traction in cryo-EM due to its speed, automation, and ease of single-particle analysis (Structura Biotechnology Inc., n.d.). However, there is minimal documentation in the literature of CryoSPARC's application for helical reconstructions of Tau fibrils, raising the question of whether CryoSPARC can match RELION's performance for helical structures.

This study provides a direct comparison of RELION and CryoSPARC for Tau fibril reconstruction, evaluating their respective capabilities from the perspective of a non-industry,

less-experienced user. By examining CryoSPARC as a potential alternative, this research seeks to determine whether it can offer a more accessible and efficient method compared to RELION. While RELION has been well-established for its use in amyloid and Tau fibril reconstructions, its computational demands and complex workflow may present limitations that CryoSPARC overcomes. This comparative analysis highlights the importance of exploring alternatives, in the context of amyloid fibrils, as well as addressing existing limitations to improve both software options. Given the complexity of amyloid fibrils and their biological significance in neurodegenerative diseases, identifying a more user-friendly tool like CryoSPARC could enhance the accessibility and scalability of cryo-EM for a wider range of research applications.

Methods

This section discusses the synthesis of Tau N410M, the formation of fibrils, Cryo-EM imaging, and helical refinement in RELION and CryoSPARC. Superscripts indicate further details on methods in Notes at the end of the Methods section.

Step 1: Synthesizing the Tau

Semi-synthetic N410M Tau fibrils were created in April 2024 by our collaborators in the Walczak Lab (Walczak Lab, n.d.) of the chemistry department at the University of Colorado-Boulder. They chemically synthesized a peptide corresponding to Tau residues 291-441 to allow for the incorporation of an N-linked glycosylation at asparagine 410 (N410), at which a mannose-containing glycan was enzymatically attached. The unmodified N-terminal portion of the protein, consisting of residues 2-290, was expressed recombinantly in *E. coli*. The two segments were chemically ligated, covalently linking the two segments, resulting in a full-length 2N4R Tau protein with the desired N410 mannose glycosylation (Powell et al., 2025).

Step 2: Fibril Preparation[1]

Tau was incubated in wells consisting of 20 μM Tau N410M (6.48 μL), 5 μM heparin (3.18 μL), 25 mM HEPES (4.29 μL), 5 μM DTT (1.75 μL), 50 mM NaCl (1.75 μL), 25 mM HEPES (17.55 μL) and left at 37° C for 72 hours.

Step 3: Cryo-EM Imaging

Tau fibrils were vitrified on a GP2 on C-flat thick 2/2 carbon-copper grids, then sent to Stanford University for imaging on their Titan Krios Beta (Thermo Fisher Scientific) at the

SLAC S^2C^2 cryo-EM center (Stanford-SLAC Cryo-EM Center, n.d.). Imaging was conducted with a 5-second blot time.

Imaging Method	single-particle
Imaging Software	EPU
File Format	.tif
Super Resolution	No
Angstrom per Pixel	0.86
Dose per Frame	1.25
Total Dose	50
Frame Duration (sec/frame)	0.0475
Exposure Time (sec)	1.76
objective_aperture/inserted	Yes
objective_aperture/size	100
Slit Size (eV)	20
Defocus	-1 to -2.4

Fig. 3 Imaging parameters.

Step 4: Helical Reconstruction

Helical reconstruction was performed in both CryoSPARC and RELION, following their respective helical processing tutorials. CryoSPARC's helical pipeline was used, following their helical processing tutorial from their structural determination program (Structura Biotechnology Inc., n.d.). The RELION reconstruction was performed following the process outlined in Lövestam & Scheres (2022) as a modification of the RELION SPA tutorial.

4.1: preprocessing. Movie frames were imported with the imaging parameters in **Fig. 1** along with an accelerating voltage of 300 kV and a spherical aberration of 2.7 mm in both software programs.

4.2: motion correction.

- CryoSPARC: Patch Motion Correction was run using default parameters.
- RELION: Motion correction was performed using MOTIONCOR2, with the following parameters:
    - Dose per frame: 1.25 e/^{2}
    - Number of patches (X,Y): 5,5
    - Binning factor: 1

4.3: CTF estimation. Patch Contrast Transfer Function (CTF) Estimation was conducted in CryoSPARC using default parameters, run on raw, non-dose-weighted micrographs for better contrast. In both software packages, the algorithm for CTF estimation divides each micrograph into overlapping patches and estimates the CTF locally for each patch. This approach is effective for tilted, bent, or deformed samples (Structura Biotechnology Inc., n.d.). CryoSPARC uses its built-in CTF estimation algorithm to determine the CTF parameters. The software analyzes the Thon rings in the power spectrum of each micrograph to estimate key parameters like defocus, astigmatism, and resolution limits (Vulović et al., 2010). CTF estimation was performed in RELION using CTFFIND 4.1 on default parameters.

4.4: curate exposures.

- CryoSPARC: The Manually Curate Exposures job was used to review and selectively retain high-quality micrographs. This tool allows users to visually inspect CTF fits, motion trajectories, and exposure statistics, enabling the manual removal of poor-quality micrographs. Micrographs can also be individually accepted or rejected. For this dataset, exposures with a CTF fit score of under 6 Å were removed.

- RELION: Unlike CryoSPARC, RELION does not have an equivalent interactive curation tool. Instead, Subset Selection was run with a maximum CTF fit of 5, comparable to setting the CTF fit threshold on CryoSPARC to 5. This removed only marginally (less than 100) more micrographs than Manually Curate Exposures on CryoSPARC.

4.5: manual particle picking. To generate templates for autopicking, manual picking was performed in both software programs. For this portion of the study, we referenced micrographs from this publication (Lövestam & Scheres, 2022) whilst selecting filaments, as fibrils may become damaged during sample preparation or be straight filaments that we aim to exclude (**Fig. 2,** C), the inclusion of which may lead to processing failures. Filaments that were swollen (**Fig. 2,** B) were also avoided.

- CryoSPARC:
    - 200 fibrils were manually picked along their entire length (see **Fig. 6**). Overlapping filament segments were used while avoiding areas of crowding or intersection points.
- RELION:
    - RELION's start-end coordinate method was used. RELION Autopicker has a micrograph limit rather than a fibril limit, so we selected fibrils from ~150 micrographs, choosing 1-10 fibril segments per micrograph.

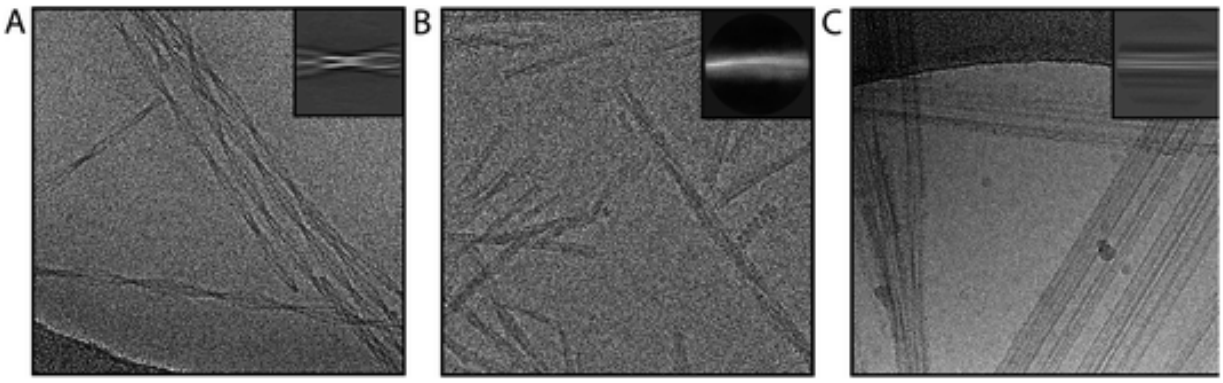

Fig. 4 Examples of good filaments (A), swollen filaments (B), and non-twisting ribbons (C).

4.6: particle extraction. After manually picking, particles were extracted with a box size of 1536 pixels, then downscaled to 512 pixels in both software programs. In RELION, extraction was performed with three unique asymmetrical units per particle to determine how many particles were extracted along the filament. The default value of 3 allowed for a good number of particles with appropriate inter-particle spacing.

4.7: 2D classification and averaging of manual picks. 2D classification and averaging were performed in both CryoSPARC and RELION to assess data quality, to eliminate suboptimal particles, and to detect the presence of multiple filament types (Lövestam & Scheres, 2022). Both software packages were run using default parameters and following tutorial parameters with specific modifications detailed below:

Parameter	CryoSPARC Settings	RELION Settings
Number of Classes	50	100
CTF Correction	Default	Ignored until first peak
Optimization Method	Default	EM
Regularization Parameter (T)	Default	2.0
Number of EM Iterations	N/A	50

Mask Diameter	N/A	1000
Angular Sampling (°)	N/A	1.0°
Offset Search Range (px)	N/A	5.0
Offset Search Step	N/A	1.0
Tube Diameter (Å)	N/A	200 Å
Angular Search Range (°)	N/A	6.0°
Helical Rise (Å)	N/A	4.75 Å (Lövestam & Scheres, 2022)

CTF Correction: Default CryoSPARC CTF correction was used, while RELION applies CTF correction with the option to ignore CTFs until the first peak, which enhances contrast and can improve 2D classification in low signal-to-noise ratio datasets.

Optimization Methods: RELION used Expectation Maximization (EM) for helical data.

4.8: selection of 2D classes. In the selection of 2D classes, poorly resolved classes which lacked cross-over features or twist were excluded, while high-resolution classes displaying potential helical patterns were selected. These 2D classes were used as input to the Autopicker software.

4.9: filament picking.

- CryoSPARC: Filaments were picked using the Template Picker job with default parameters, including a filament diameter of 200 Å and a separation distance of 0.25 (this setting is equivalent to using 70 asymmetrical units with the default separation distance of 0.25).
    - The Inspect Particle Picks job was then used to refine selections, allowing for the removal of false positives, contaminants, or highly bent filaments by adjusting the Power Score and NCC sliders (**Fig. 14**)

- RELION: To enhance filament selection, Topaz, a deep-learning-based particle picker, was implemented. The Topaz executable is integrated into RELION, allowing a neural network to be trained to identify particles resembling manually selected ones. The following parameters were used:
    - Particle diameter: 200 Å
    - Train on a set of particles: Yes
    - In-plane angular sampling: 2°
    - Pick 2D helical segments: Yes
    - Tube diameter: 200 Å
    - Minimum length: -1 Å
    - Maximum Curvature: 0.4 kappa[2]
    - Number of unique asymmetrical units: 3 (overlap between segments, comparable to CryoSPARC's interparticle separation distance)
    - Helical rise: 4.75 Å
    - Trained model to pick particles: Now that the model is made, Topaz can be used to pick filaments. Some specifications were made:
        - Threshold, Hough length (Å): -4, -1[3]
        - Picking threshold: 0.05

4.10: extracting micrographs. Micrographs were extracted in both software programs with an extraction box size of 1536 pixels, ensuring consistency.

4.11: 2D class averaging after filament picking. 2D class averaging was iterated several more times in both software programs to refine the dataset by selecting high-quality particle classes. Increasing the class size for these runs improved resolution and reduced noise.

2D class averaging was performed four more times with a class size of 200 in CryoSPARC. 2D class averaging was performed six more times with a class size of 150 in RELION, as the RELION Autopicker identified a significantly higher number of particles, requiring further parsing.

RUN 1 parameters:

- CryoSPARC: A 2D class size of 200 and default parameters were used (**Fig. 16,17**). The five best classes were selected (**Fig. 18**).
- RELION: A 2D class size of 150, 25 EM iterations, and a regularization parameter of 2 were used (**Fig. 18**).

FINAL RUNS:

- CryoSPARC: A 2D class size of 200 and default parameters were used (parameters used for runs 1-4). The nine best classes were selected (**Fig. 21**).
- RELION: A 2D class size of 150, 25 EM iterations, a regularization parameter of 2, ignore CTF before first peak (parameters used for runs 1-6).

4.12: 3D model reconstruction.

- CryoSPARC: To produce an initial model, the Ab-Initio Reconstruction job was used since it provides several different views along the helix and often results in a better initial model. Next, the initial volume was run through the Homogeneous refinement job with default symmetry parameter of C1. Next, a Helical Refinement job constructs the filament from the particles without applying symmetry and uses the standard maximum likelihood optimization.
    - Helical Refinement was run with the following parameters:
        - Helical rise estimate: 4.5 Å

- Use non-uniform refinement: Yes

- The Symmetry search utility was employed to assess symmetry present in the initial reconstruction. Since no symmetry was imposed during the initial reconstruction, evaluating how well this new volume aligns with various symmetry parameters provides an unbiased assessment of the inherent symmetry present in the dataset.
  - The local minima output provides the parameters for the new reconstruction (**Fig. 24**). Symmetry search was run with the following parameters:
    - Rise: 3.5, 5.5 Å
    - Twist: -30, 30°
- Symmetric Helical Refinement: when estimates for symmetry parameters are known, it is recommended to run a helical refinement with the estimated twist (°) and rise (Å) as input parameters. Enforcing symmetry allows for the enhancement of the effective signal within the dataset and application of a strong structural constraint to the reconstruction. Outputs from row No. 0 from **Fig. 24** were used to generate the model:
  - Twist= 0.1176° Rise= 3.5 Å
- Inverted Reconstruction Correction: in most cases, left-handed alpha helices are unexpected and suggest that the overall reconstruction has an inverted handedness. This occurs because the handedness of a cryo-EM map is inherently ambiguous—particles can reconstruct a density map just as easily with its mirrored image. Reversing the sign of the helical twist is equivalent to flipping

the handedness of the reconstruction. To do this, the Volume Tools job was run with the following parameter:

- Flip hand: Yes

- Final Helical Reconstruction (**Fig. 25, 27**): a final reconstruction was obtained from the symmetry search parameters with the same rise, but inverted twist:
  - Twist= -0.1176° Rise= 3.5 Å

- RELION uses a gradient-driven algorithm to degenerate an initial 3D model from the 2D particles (RELION, n.d.) using the newly generated initial 2D model (**Fig. 23**) as the reference map to better construct a 3D model. The initial 2D model is generated using the helix_inimodel_2d, a RELION utility designed to produce a continuous 2D template for helical structures.

  A 3D model was constructed (**Fig. 27**) with the following parameters:

  - Symmetry: C1[4]
  - CTF-correction: Yes
  - Ignore CTFs until first peak: Yes
  - Mask diameter: 450 Å[5]
  - Use blush regularization: Yes[6]
  - Use finer angular sampling faster: No[7]
  - Do helical reconstruction: Yes
  - Apply helical symmetry: Yes
  - Initial twist (°), rise (Å): 0.45, 4.75[8]
  - Do local searches of symmetry: No

Notes.

1. Heparin is a glycosaminoglycan (GAG) that is negatively charged due to sulfate and carboxyl groups and is commonly used to induce Tau aggregation *in vitro*. Heparin participates in the rate-limiting step of aggregation (Ramachandran et al., 2011). DTT (dithiothreitol) detergent was used as a chemical compound commonly used to reduce disulfide bonds in proteins (Konigsberg, 1972), helping to unfold them and prevent aggregation while still allowing fibrils to form. HEPES (4-(2-hydroxyethyl)-1-piperazineethanesulfonic acid) buffer was used to maintain a stable pH at low temperatures (G-Biosciences, 2023).
2. Maximum curvature of 0.4 allows flexibility in filament shape.
3. Useful for detecting straight lines, and allows for the detection of amyloids due to their faint contrast, orientation, and sometimes shorter segments.
4. C1 is the default parameter used since the symmetry is unknown.
5. Binning size is 512 Å, so a radius of 450 Å region of interest is reasonable to exclude background noise whilst preserving the structural information.
6. Blush regularization is useful for suppressing noise and maintaining the structural integrity.
7. Sped-up calculations have not been tested on reconstruction quality.
8. RELION does not have symmetry search utility so initial twist was inputted based on previous papers (Lövestam & Scheres, 2022).

Results

Data Processing Comparison Using CryoSPARC vs. RELION for Helical Reconstructions

Manual Picking (refer to **Methods 4.5**): Differences in micrograph quality, fibril representation, and selection strategies were observed between the two software programs. As shown in **Fig. 6**, CryoSPARC has users select the entire length of the fibril and RELION employs a start-end coordinate method, allowing for precise centering and improved particle selection. This method provided more control over particle alignment and extraction. In CryoSPARC, particles are only extracted from the selected picks, whereas in RELION, the amount extracted can be altered via the asymmetric units count.

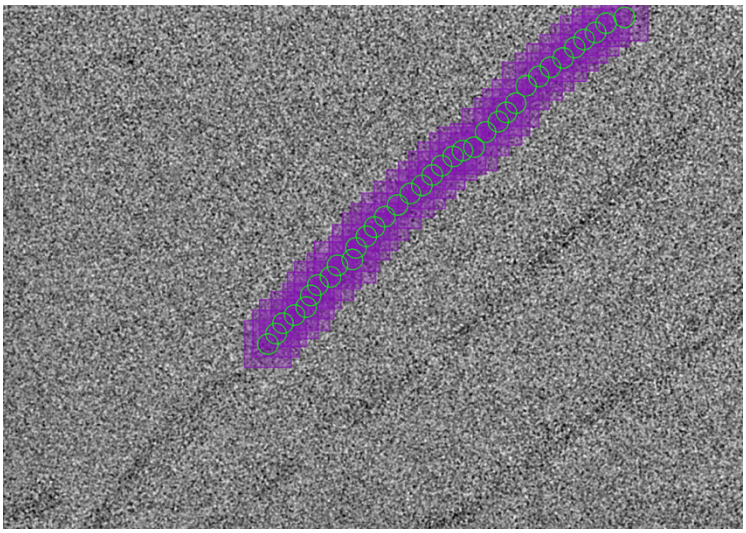

Fig. 6 Manual picking process in CryoSPARC.

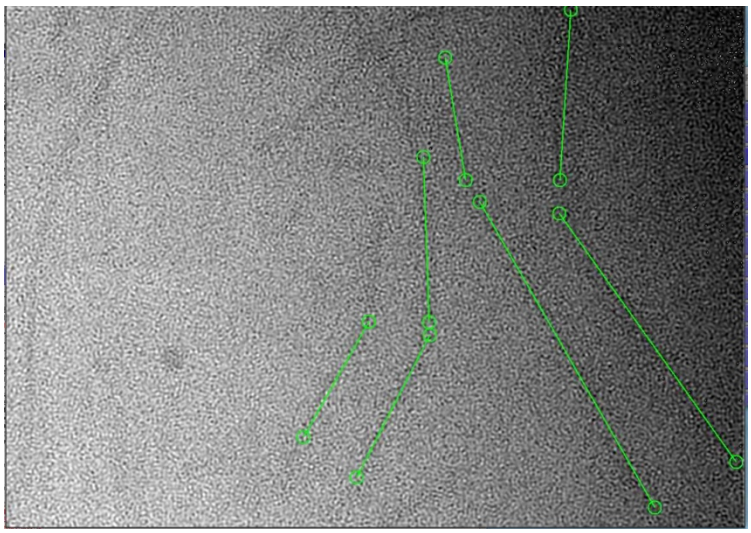

Fig. 7 Manually picking in RELION using start-end coordinates (Poliyenko, preliminary data).

Fig. 8 displays examples of well-defined fibrils, demonstrating clear structural integrity and twisting against the background noise**. Fig. 9** presents a poor-quality micrograph where fibril definition is less distinct. Such differences in micrograph quality impact particle selection and downstream processing, influencing the final reconstruction.

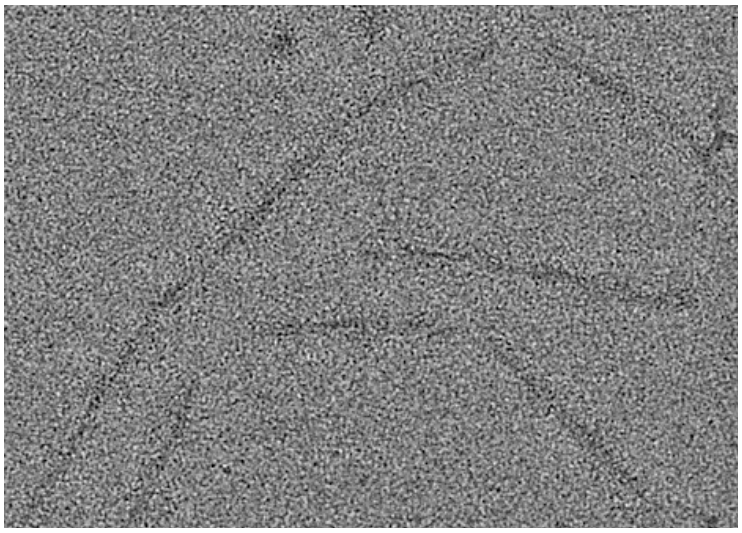

Fig. 8 Examples of representative fibrils from our dataset in CryoSPARC.

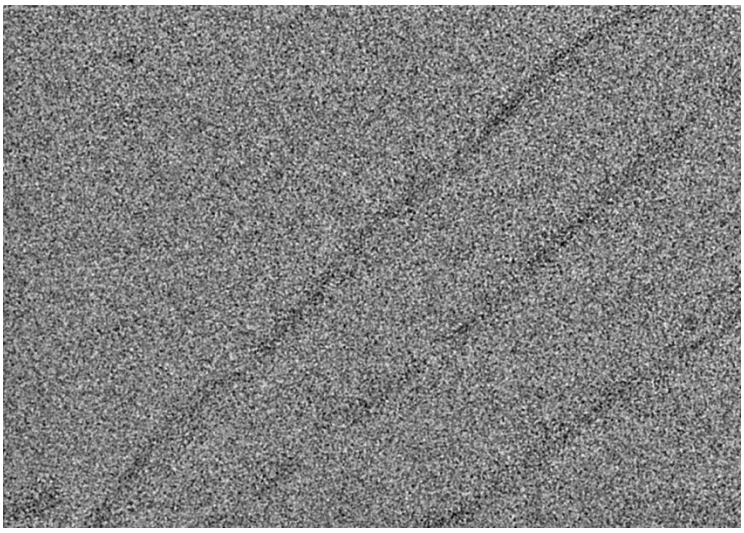

Fig. 9 Examples of a poor-quality micrograph from our dataset in CryoSPARC.

2D Classification (refer to **Methods 4.7**): In **Fig. 11**, RELION outputted better-quality and higher-resolution classes from 2D classification than CryoSPARC did in **Fig. 10**. CryoSPARC's 2D classification operates with a high degree of automation, limiting user access to certain parameters such as offset search range, mask diameter, or helical rise (CryoSPARC Discuss, 2020). RELION offers extensive user control during 2D classification, and this flexibility allows users to adjust parameters better suited for helical reconstruction.

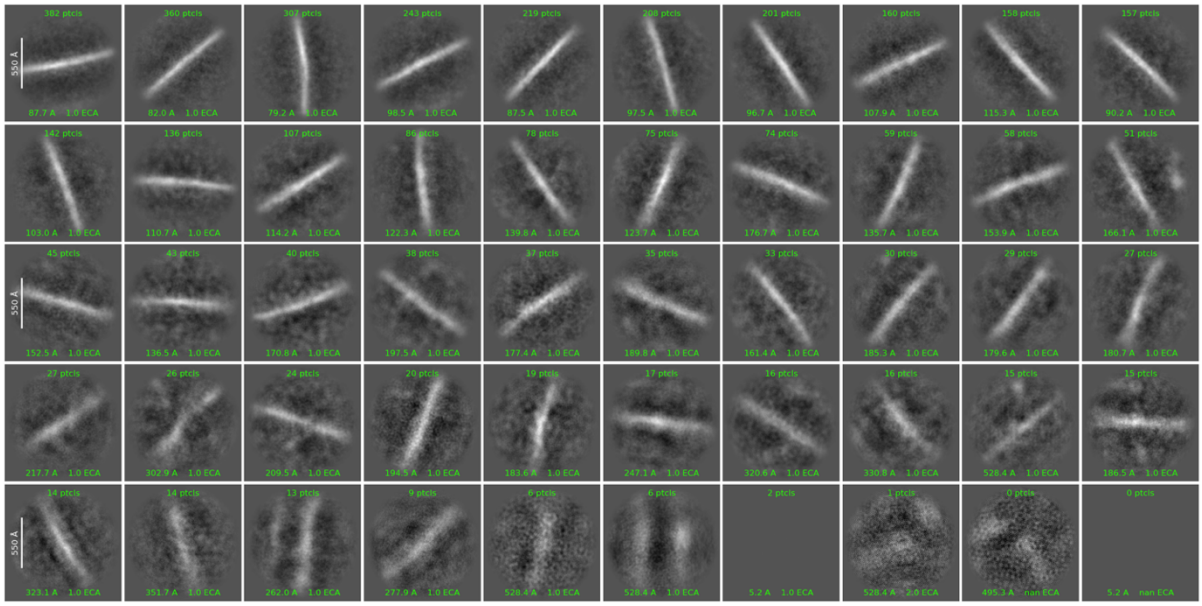

Fig. 10 Output 2D classes from manual picks in CryoSPARC. (Scale bar=550 A).

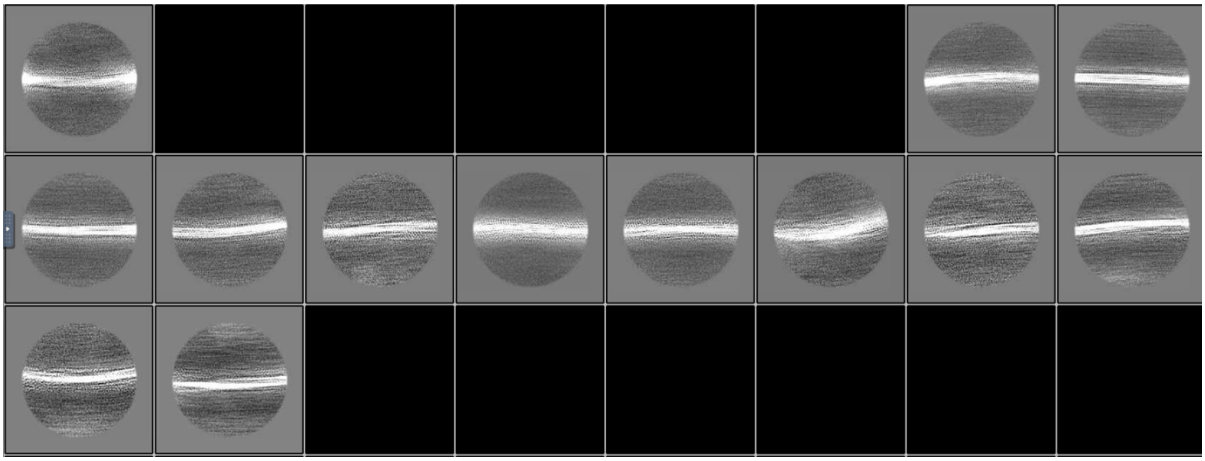

Fig. 11 Output 2D classes from manual picks in RELION. Fibril lengths are ~1000 A (Poliyenko, preliminary data).

Overall, CryoSPARC's default settings streamline its 2D classification, whereas RELION allows for more extensive manual parameter customization for optimal helical results. Also, despite providing RELION with a command to make 100 classes, it did not fill all of them with particles (as depicted by black squares in **Fig. 11**), suggesting greater confidence in particle classification.

The selected 2D classes, shown in **Fig. 12** and **Fig. 13,** indicate well-preserved cross-over helical structures. The estimated resolution of the selected 2D classes in CryoSPARC was ~95 Å (see **Fig. 12**). Selected RELION classes showed clear helical striations with a much higher estimated resolution compared to CryoSPARC, ranging from ~13.5 Å to ~17.6 Å (see **Fig. 13**).

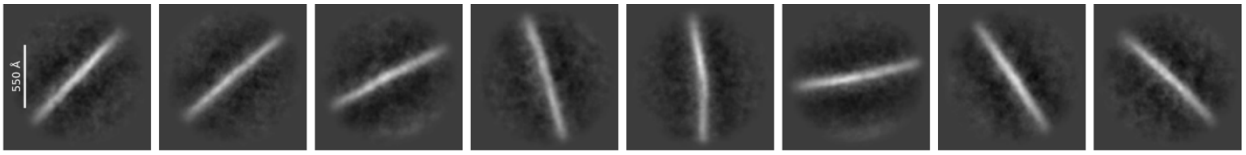

Fig. 12 Selected 2D class output from CryoSPARC with an estimated resolution of ~95 Å. (Scale bar=550 A).

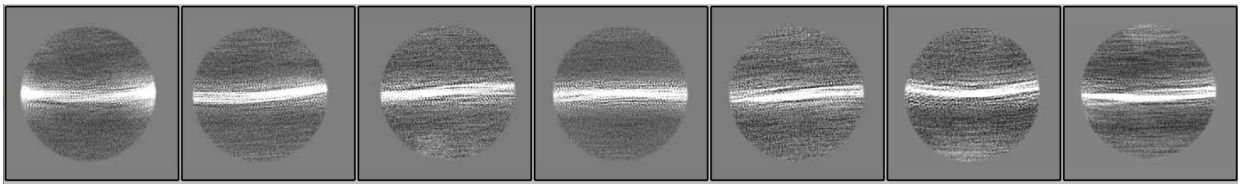

Fig. 13 Selected 2D class output from RELION with an estimated resolution of ~13.5 Å (left panel) to ~17.6 Å (right panel). Fibril lengths are ~1000 A (Poliyenko, preliminary data).

Filament Picking (refer to **Methods 4.9**): CryoSPARC and RELION employ different approaches facilitate filament picking. CryoSPARC uses the Template Picker job then an Inspect Picks job, while RELION recommends using Topaz.

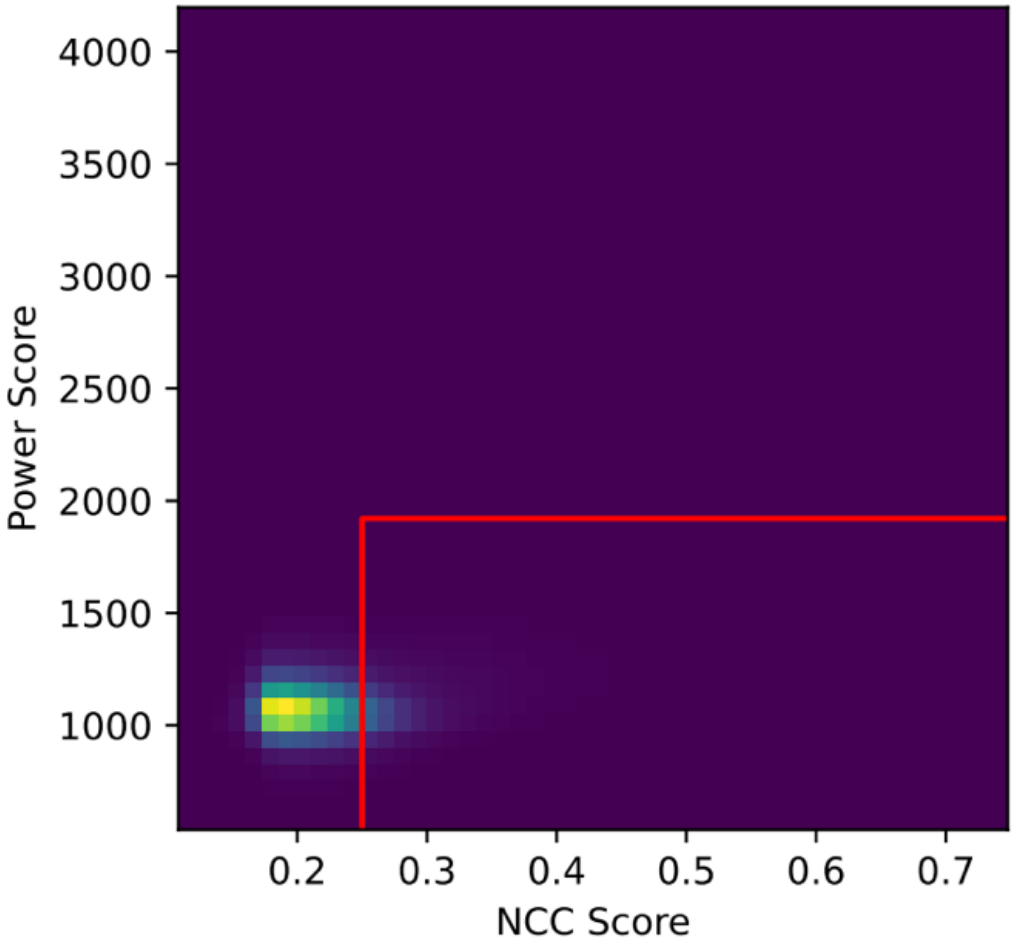

Fig. 14 Final selected thresholds from the Inspect Particle Picks job in CryoSPARC.

Through the Inspect Picks job, 12,463 micrographs and 1,426,051 particles were accepted, while 6,156,234 particles were excluded, with an average of 114 picks per micrograph.

- Accepted particles met the following criteria:
  - NCC score > 0.250
  - Local power > -440.000
  - Local power < 1921.000

The Inspect Particle Picks job was then used to refine selections, allowing for the removal of false positives, contaminants, or highly bent filaments by adjusting the Power Score and NCC sliders (**Fig. 14**).

RELION integrates Topaz, a deep-learning-based particle picker, allowing users to train a neural network to identify particles resembling manually selected ones and enhance filament selection.

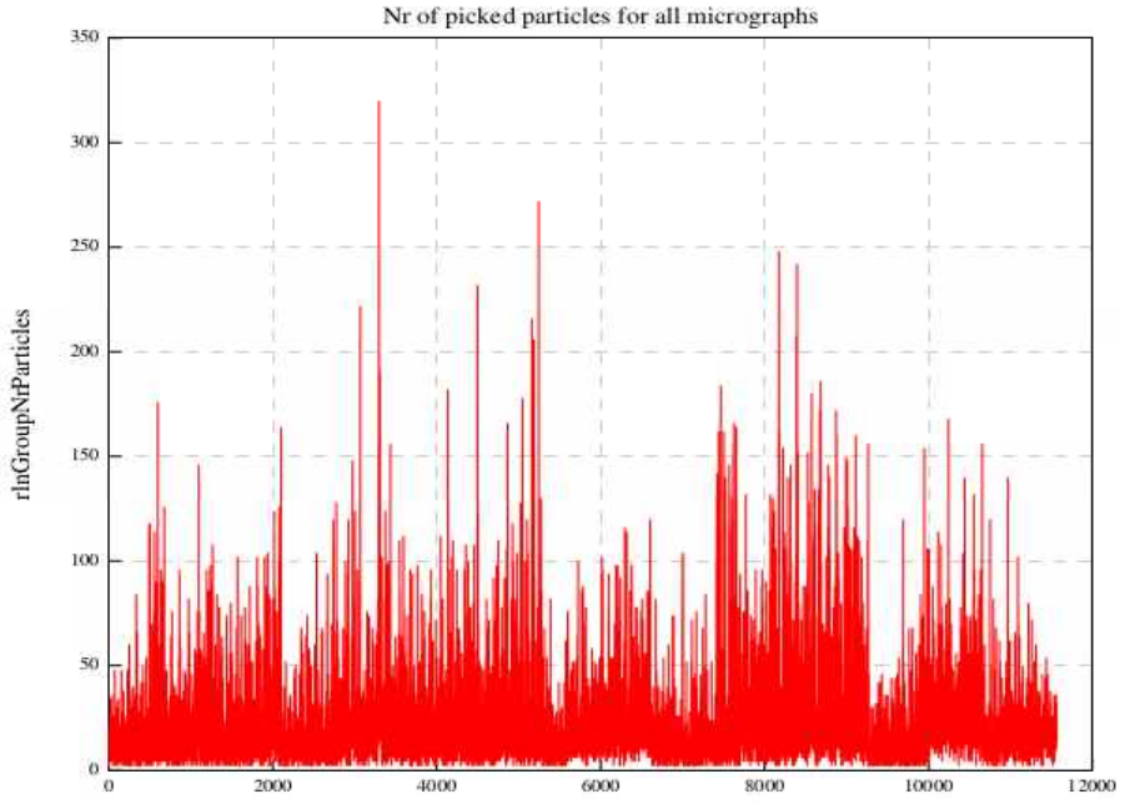

Fig. 15 Number of picked particles per micrograph for all micrographs in RELION. X-axis is micrograph number. (Poliyenko, preliminary data).

2D class averaging after filament picking (refer to **Methods 4.11**): Following filament picking, 2D classifications provide insight into structural variability and resolution of the dataset. **Fig. 16** presents an overview of the 200 output classes from the first run in CryoSPARC, highlighting a range of fibril conformations and resolutions. From these, five of the highest-quality classes were selected, as shown in **Fig. 17.**

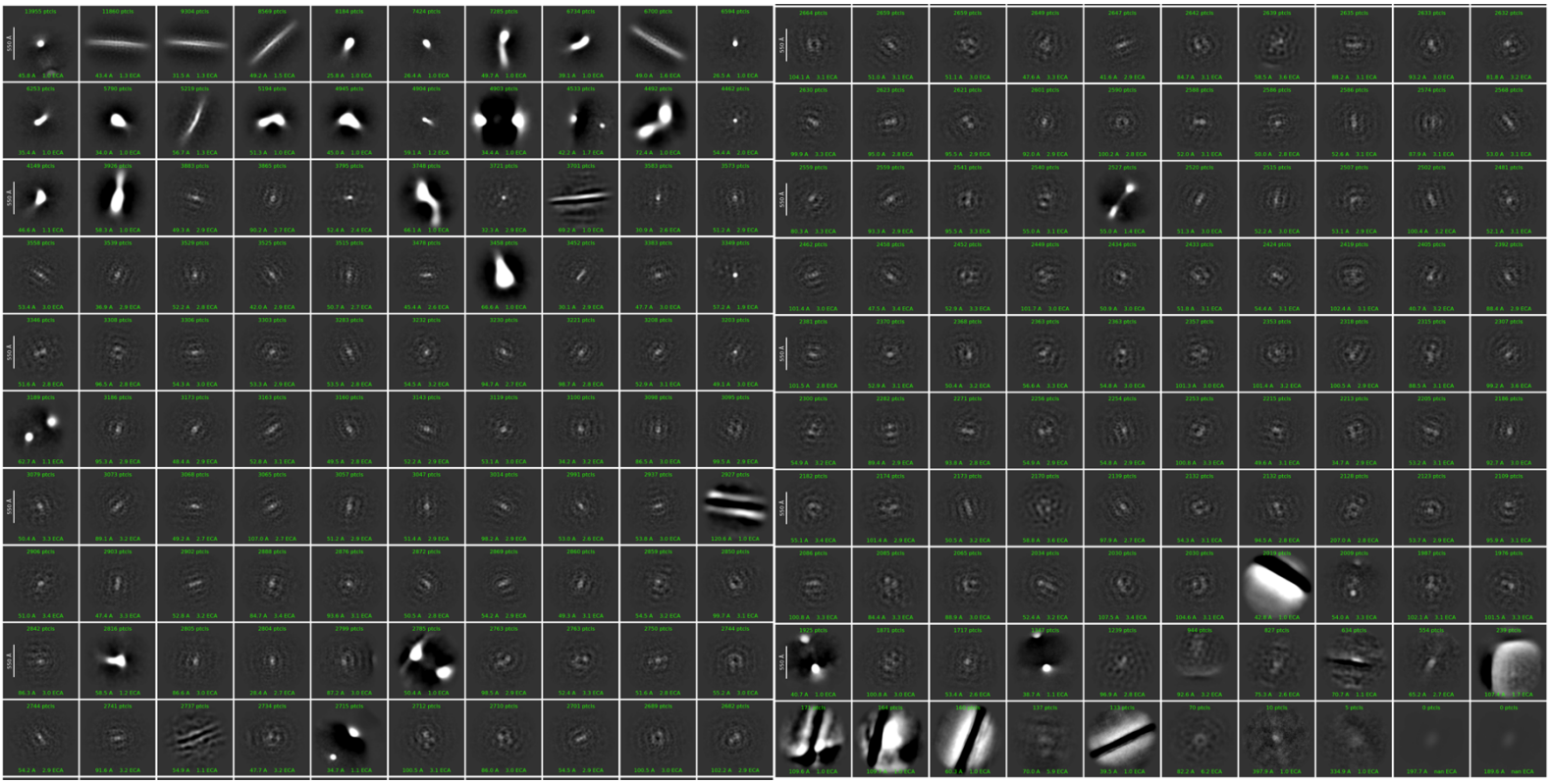

Fig. 16 Example output 2D 200 classes from CryoSPARC in run 1 (run on default parameters) with resolution ranging from 25.8 Å to 397.9 Å. (Scale bar=550 A).

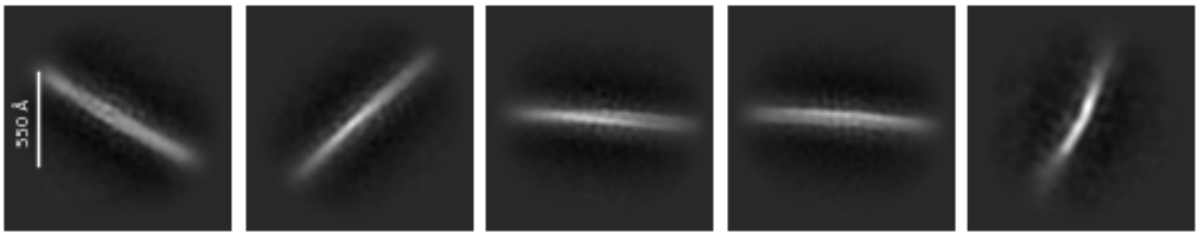

Fig. 17 Five best selected classes from CryoSPARC in run 1. (Scale bar=550 A).

Fig. 18 presents an overview of the output classes from RELION after the first run as well.

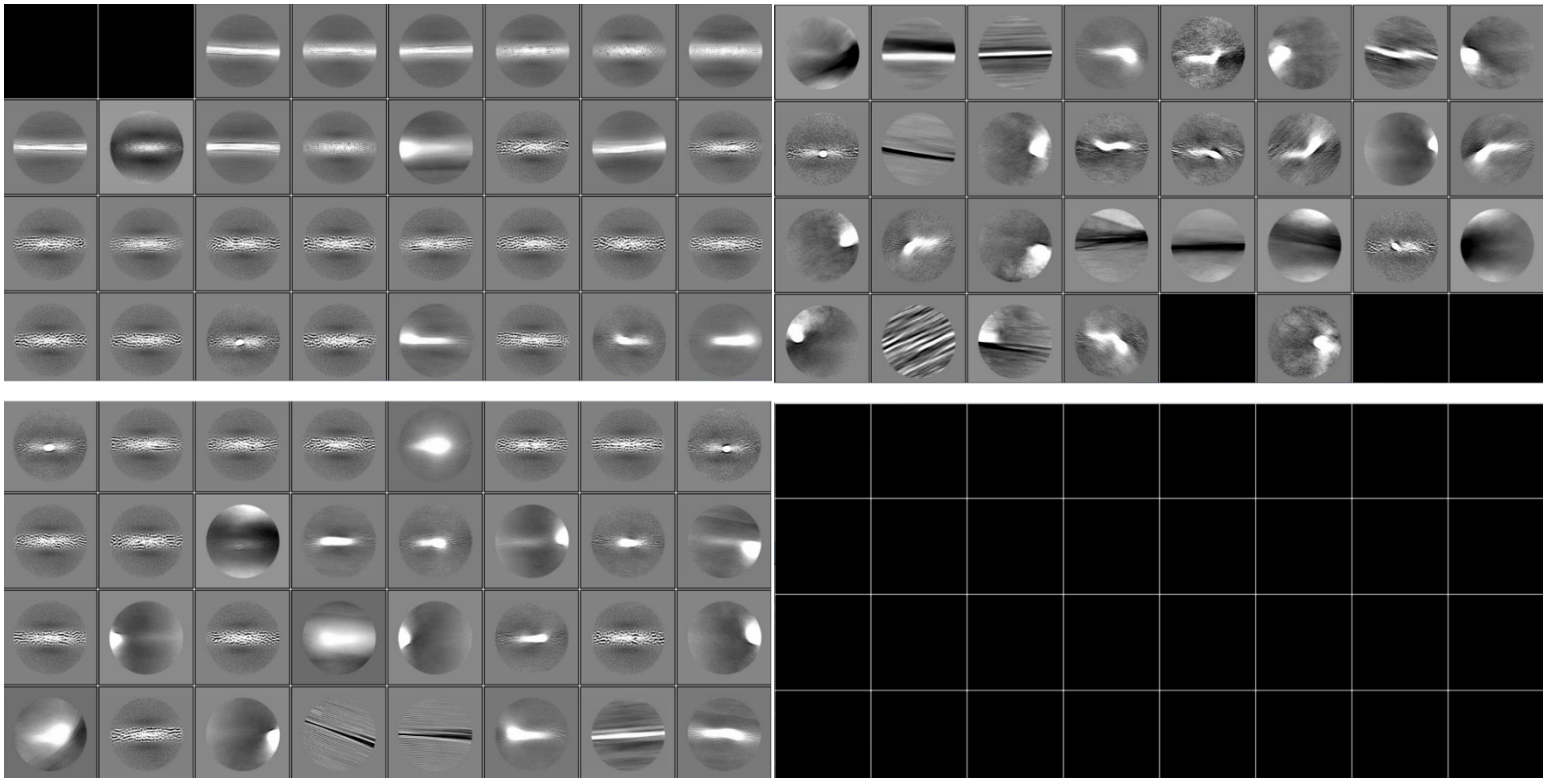

Fig. 18 Output 2D classes from RELION in run 1 and sorted in order of estimated resolution. Notably, RELION did not fill all classes with particles. Fibril lengths are ~1000 A (Poliyenko, preliminary data).

2D class averaging was run several times to ensure the best-quality classes and reduced noise. 2D class averaging was performed four more times with a class size of 200 in CryoSPARC. 2D class averaging was performed six more times with a class size of 150 in RELION. The best classes selected in CryoSPARC are shown in **Fig. 19**, while those from RELION are shown in **Fig. 20.**

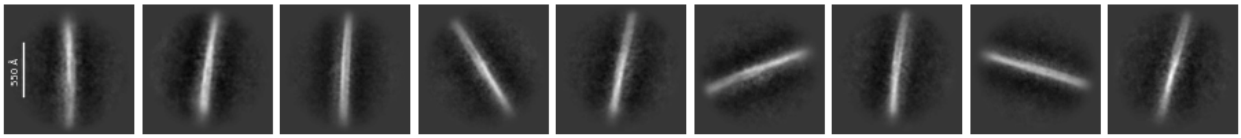

Fig. 19 Selected classes in CryoSPARC from run 4. (Scale bar=550 A).

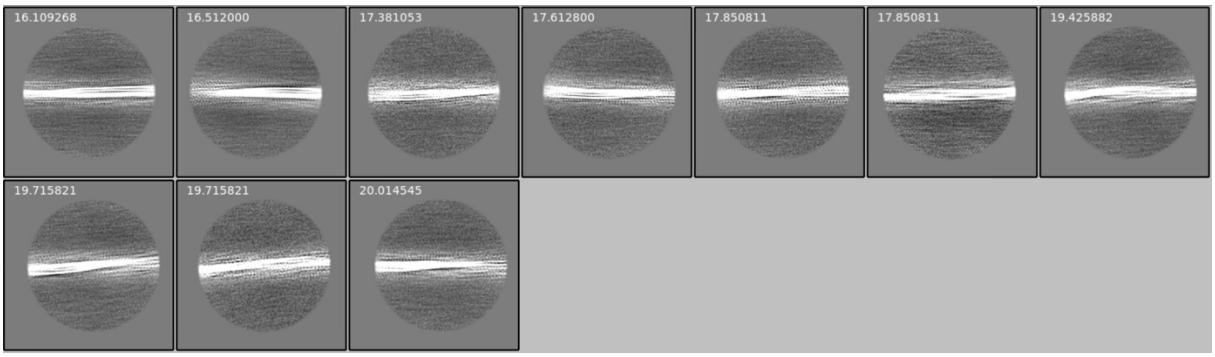

Fig. 20 Selected classes in RELION from run 6. Fibril lengths are ~1000 A (Poliyenko, preliminary data).

The iterative 2D class averaging process in both CryoSPARC and RELION allowed for the refinement of fibril structures, reducing noise and enhancing resolution, but RELION yielded higher-resolution class averages with distinct fibril cross-over patterns.

RELION also has the ability to form an initial 2D model (**Fig. 23**), allowing users to use this as a reference for a 3D model, rather than just the selected 2D classes. However, quite inconveniently, this must be done externally via a script coded by the user and run from the command line, and input back into RELION as an input for the initial 3D reconstruction job.

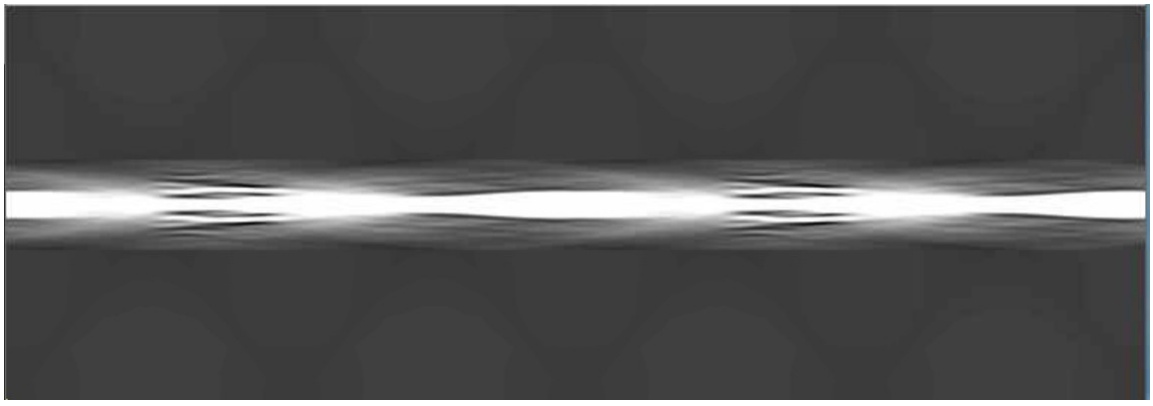

Fig. 23 Initial continuous 2D model from RELION (Poliyenko, preliminary data).

3D model reconstruction (refer to **Methods 4.12**): The Symmetry search utility in CryoSPARC was used to assess symmetry in the initial reconstruction, as no symmetry was imposed initially. The local minima output provides the parameters for the new reconstruction (**Fig. 24**).

Showing the 20 best local minima.

No.	p (A)	n	dz (A)	dphi (deg)	mse
0	1.071e+04	3.060e+03	3.500e+00	+1.176e-01	3.499e+02
1	7.101e+01	1.291e+01	5.500e+00	-2.788e+01	6.067e+02
2	6.909e+01	1.291e+01	5.351e+00	-2.788e+01	6.070e+02
3	7.162e+01	1.302e+01	5.500e+00	+2.765e+01	6.071e+02
4	6.828e+01	1.291e+01	5.288e+00	-2.788e+01	6.072e+02
5	2.370e+02	4.310e+01	5.500e+00	+8.353e+00	6.073e+02
6	2.240e+02	5.016e+01	4.465e+00	+7.176e+00	6.074e+02
7	6.968e+01	1.302e+01	5.351e+00	+2.765e+01	6.075e+02
8	6.886e+01	1.302e+01	5.288e+00	+2.765e+01	6.076e+02
9	2.306e+02	4.310e+01	5.351e+00	+8.353e+00	6.076e+02
10	2.279e+02	4.310e+01	5.288e+00	+8.353e+00	6.078e+02
11	2.153e+02	5.016e+01	4.292e+00	+7.176e+00	6.079e+02
12	6.590e+01	1.302e+01	5.061e+00	+2.765e+01	6.081e+02
13	6.301e+01	1.291e+01	4.880e+00	-2.788e+01	6.082e+02
14	6.539e+01	1.302e+01	5.022e+00	+2.765e+01	6.082e+02
15	6.251e+01	1.291e+01	4.841e+00	-2.788e+01	6.083e+02
16	6.477e+01	1.302e+01	4.975e+00	+2.765e+01	6.083e+02
17	6.230e+01	1.291e+01	4.825e+00	-2.788e+01	6.083e+02
18	6.457e+01	1.302e+01	4.959e+00	+2.765e+01	6.083e+02
19	6.170e+01	1.291e+01	4.778e+00	-2.788e+01	6.084e+02

Fig. 24 20 best local minima provided from the Symmetry Search job in CryoSPARC.

The first column was used for input parameters for the final reconstruction as they are supposed to provide the symmetry for the final reconstruction. The mse values are very similar for all 20 local minima, suggesting that it got trapped in a suboptimal solution, which can lead to an inaccurate 3D model.

In CryoSPARC, a final reconstruction was obtained from the symmetry search parameters with the same rise of 3.5 Å, but inverted twist of -0.1176°. **Fig. 25** displays the final 3D reconstruction in the program Chimera.

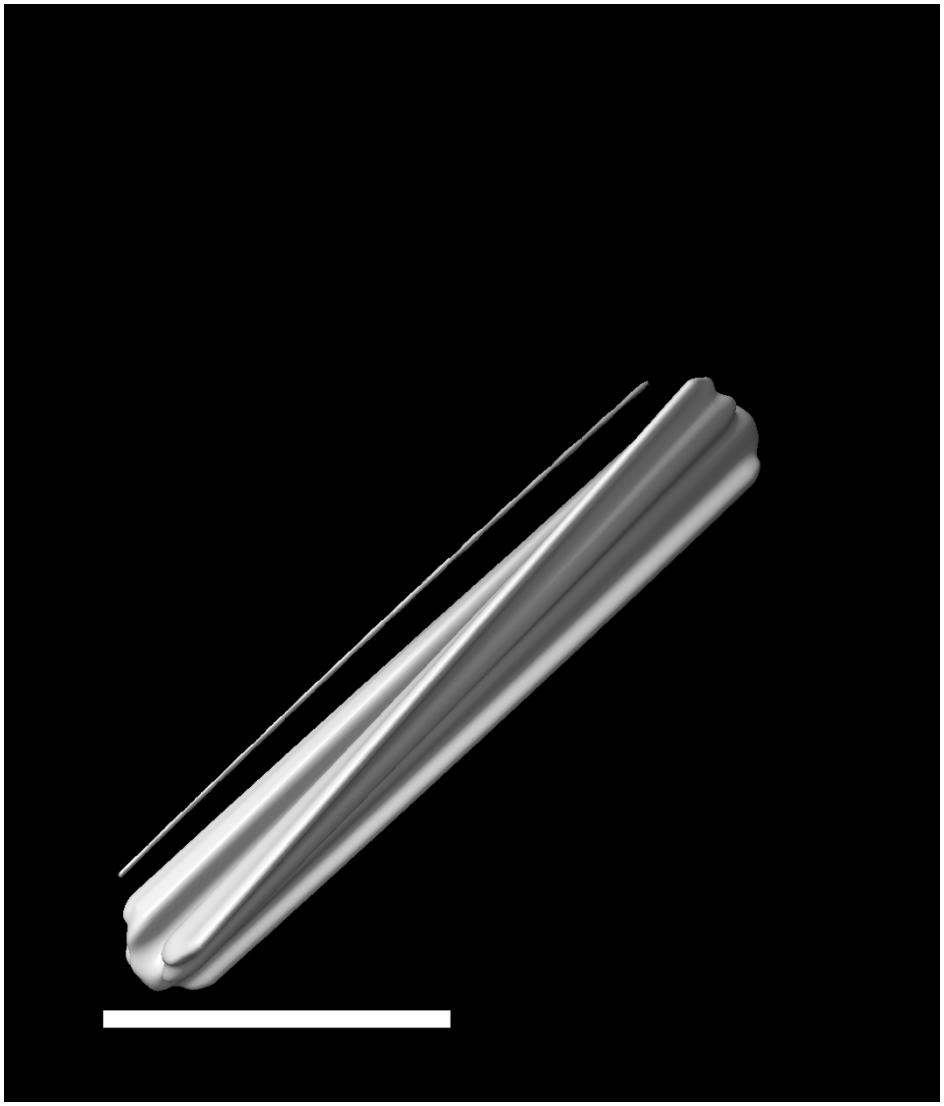

Fig. 25 Final 3D map from CryoSPARC viewed in the program Chimera. (Scale bar=500 A).

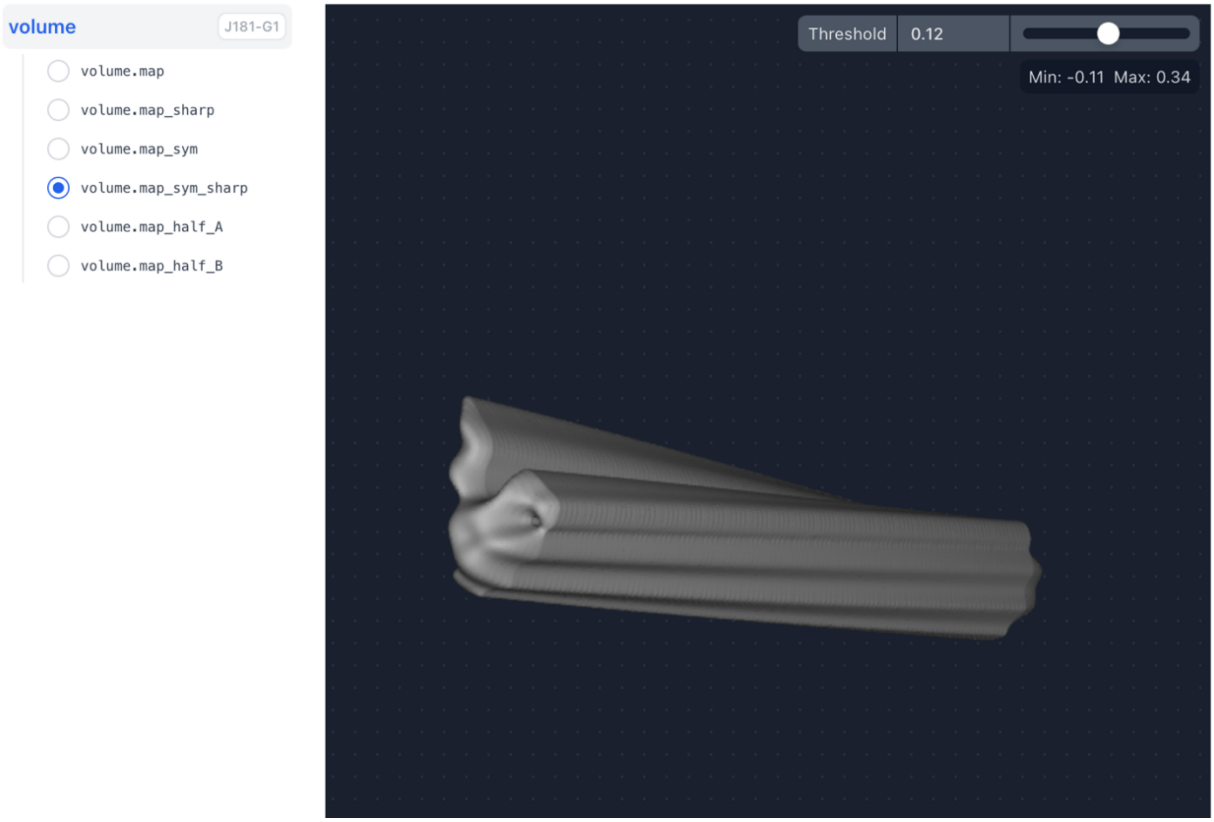

Fig. 26 Built-in tool to view final volume in CryoSPARC.

RELION uses a gradient-driven algorithm to generate an initial 3D model from the 2D particles using the newly generated initial 2D model (**Fig. 23**) as the reference map to better construct a 3D model. A 3D model was constructed and shown in **Fig. 27**.

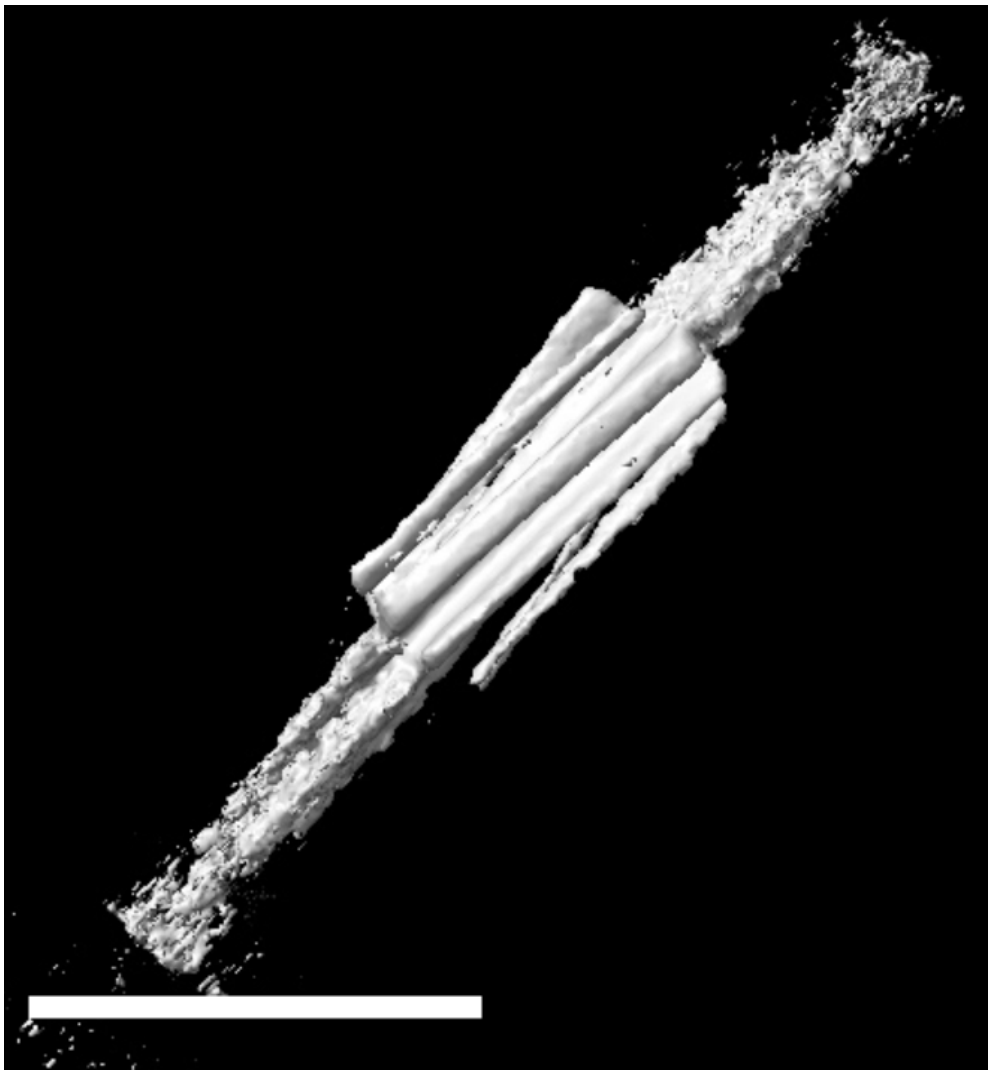

Fig. 27 Final 3D reconstruction from RELION in the program Chimera. (Scale bar=500 A). (Poliyenko, preliminary data).

The final 3D reconstruction generated by RELION (**Fig. 27**) yielded a superior structure compared to CryoSPARC (**Fig. 25**), exhibiting higher accuracy and distinct fibril-like features with beta-like figures at the core.

Discussion

There are many significant distinctions between the helical reconstruction pipelines of CryoSPARC and RELION, which result in diverse outcomes. Their differences in preferred methods, steps, and automation play a key role in the final helical reconstruction.

Manual particle picking (refer to Sections 4,5 & 9 from Results). RELION lacks tools like the Inspect Particle Picks job or Manually Curate Exposures job that CryoSPARC encompasses, allowing for more interaction and flexibility in curating exposures manually when dealing with challenging datasets. CryoSPARC lacks the ability to use start-end coordinates in manually picking particles, which results in fewer precise particle picks. Thus, RELION may provide the user with higher ease-of-use during the manual picking step, while losing control over manually excluding micrographs beforehand, relying on longer 2D class averaging to rule out poor particles, compared to being able to rapidly exclude them in CryoSPARC.

Filament picking & Topaz (refer to Section 9 from Results). For filament picking in RELION, Topaz is highly recommended. Topaz can be trained to specific filament types and works well for detecting filaments in noisy or low-resolution micrographs, making it particularly useful for helical structures like amyloid fibrils. CryoSPARC, while offering Topaz as an option—unfortunately requiring access to a command line, which is not intrinsically provided in CryoSPARC itself—recommends its own filament-picking approach, which is considered less robust compared to RELION's integration of Topaz.

2D classification (refer to Sections 7 & 11 from Results). One of the key advantages of RELION is the continuous initial 2D model it provides from the results of 2D classification,

which is very beneficial in providing the 3D reconstruction job with more flexibility and a more accurate representation. While CryoSPARC offers 2D classification, it does not have the same continuous 2D model like RELION, which limits helical accuracy. RELION also utilizes a maximum a posteriori (MAP) expectation-maximization algorithm for 2D class averaging, incorporating Bayesian statistical modeling to improve particle alignment and classification (Scheres, 2012). This method is advantageous for Tau fibrils due to their intrinsic heterogeneity, as it better accounts for subtle structural variations (Duan et al., 2024).

Symmetry search & local minima (refer to Section 12 from Results). When working with helical symmetries, getting stuck in local minima in both software programs remains to be a major challenge when facing amyloid determination. Although previous literature describes various strategies for recognizing and avoiding this, it requires users to be especially vigilant and aware of unexpected features in the symmetry map in RELION as well (Lövestam & Scheres, 2022). In CryoSPARC, when the symmetry search results push the input rise and twist to extremes, there is a lack of clarity as to what constitutes true symmetry and this can be misleading since the twist and rise values are taken from this when making 3D reconstructions.

Final 3D reconstructions (refer to Section 12 from Results). Given the advantages of the continuous 2D model, Topaz usage, particle picking, and more robust helical refinement, RELION was able to produce overall a better-quality and higher-resolution final 3D reconstruction for helical amyloid filaments. While CryoSPARC provides impressive results in many standard SPA reconstructions, its tools for amyloid filaments are not as well-developed as those in RELION, leading to less optimized final reconstructions.

CryoSPARC acknowledges that amyloid fibrils present a challenge for final reconstructions due to the lack of specialized tools for particle picking or refinement (CryoSPARC, n.d.), but improvements to their current utilities can be made to enhance the helical reconstruction process as is. 2D classification can be enhanced by allowing for the adjustment of parameters such as angular sampling, mask diameter, tube diameter, offset search range, and estimated helical rise. CryoSPARC can benefit from integrating Topaz for picking by default because currently there exists many installation issues (CryoSPARC Discuss, 2021) and permission errors (CryoSPARC Discuss, 2020) as reported by other users. The symmetry search utility can make improvements in more reliable optimization techniques to help address this issue of getting stuck in local minima (Lövestam & Scheres, 2022). At a minimum, the CryoSPARC Guide should warn users of the capacity for the symmetry search to give 'mathematically right' solutions that do not match expectations for the structures users examine.

In summary, both CryoSPARC and RELION offer distinct advantages and challenges in the process of helical reconstruction for amyloid filaments like Tau fibrils. While RELION excels in continuous 2D modeling, filament picking with Topaz, and robust helical refinements, CryoSPARC provides valuable tools for manual particle inspection and interactive curation. The lack of specialized tools in CryoSPARC for amyloid reconstruction limits its overall performance. These limitations highlight significant potential improvements in CryoSPARC's algorithms to match RELION's capabilities while retaining a more user-friendly interface.

Conclusion

This research conclusively demonstrates RELION's superior performance over CryoSPARC in the structural determination of Tau N410M fibrils, primarily due to its advanced tools, including continuous 2D initial model generation, Topaz filament picking, and robust helical refinement techniques. These features make RELION the more effective software for reconstructing amyloid-like structures. In contrast, CryoSPARC's helical reconstruction pipeline remains limited by its lack of specialized tools for particle picking and refinement.

To enhance CryoSPARC's utility, future developments should focus on an easier integration of Topaz, improving symmetry search algorithms, and offering more flexible filament-picking methods. These advancements could significantly improve its ability to handle complex fibril structures. This research provides a foundation for future studies that could leverage CryoSPARC's strengths in helical reconstruction processing while addressing its current limitations. Improving CryoSPARC's ability to handle complex fibril structures could enhance its user-friendly interface and faster processing capabilities, leading to broader adoption within the scientific community. If optimized, importing and exporting between the two software programs could allow users to leverage the strengths of both in their reconstruction pipelines. These enhancements would facilitate the structural determination of more Tau fibrils implicated in Alzheimer's disease and other neurodegenerative diseases.

References

Alzheimer's Disease International. (n.d.). *Dementia statistics*. Retrieved from https://www.alzint.org/about/dementia-facts-figures/dementia-statistics/

Frontiers in Neurology. (2020). *The role of cryo-EM in neurodegenerative diseases*. Retrieved from https://www.frontiersin.org/journals/neurology/articles/10.3389/fneur.2020.590754/full

International Federation of Red Cross and Red Crescent Societies. (2024). *Amyloid structure determination in RELION-3.1*. Retrieved from https://pmc.ncbi.nlm.nih.gov/articles/PMC7008511/

Medical Research Council Laboratory of Molecular Biology. (n.d.). *RELION*. Retrieved from https://www3.mrc-lmb.cam.ac.uk/relion/index.php/Main_Page

National Center for Biotechnology Information. (n.d.). *Structural insights into tau fibrils*. Retrieved from https://pmc.ncbi.nlm.nih.gov/articles/PMC6225777/

Nature Medicine. (1996). *Neurodegeneration mechanisms*. Retrieved from https://www.nature.com/articles/nm0896-871#preview

Nature Methods. (2017). *Advances in cryo-EM for structural biology*. Retrieved from https://www.nature.com/articles/nmeth.4169

Nature Structural & Molecular Biology. (2024). *Recent developments in cryo-EM*. Retrieved from https://www.nature.com/articles/s41594-024-01252-3

Nature Methods. (2024). *Innovations in cryo-EM data processing*. Retrieved from https://www.nature.com/articles/s41592-024-02304-8

PubMed. (2001). *Defocus estimation in cryo-EM*. Retrieved from https://pubmed.ncbi.nlm.nih.gov/11447842/

PubMed Central. (n.d.). *The application of cryo-EM in structural biology*. Retrieved from https://pmc.ncbi.nlm.nih.gov/articles/PMC5390006/

PubMed Central. (n.d.). *New methods in cryo-EM data processing*. Retrieved from https://pmc.ncbi.nlm.nih.gov/articles/PMC10527703/

PubMed Central. (n.d.). *Tau fibril structure determination*. Retrieved from https://pmc.ncbi.nlm.nih.gov/articles/PMC7688747/

PubMed Central. (n.d.). *Cryo-EM imaging and neurodegenerative diseases*. Retrieved from https://pmc.ncbi.nlm.nih.gov/articles/PMC3975420/

PubMed Central. (n.d.). *Challenges in amyloid fibril reconstruction*. Retrieved from https://pmc.ncbi.nlm.nih.gov/articles/PMC6692637/

Science Advances. (2024). *Recent advances in cryo-EM*. Retrieved from https://www.science.org/doi/10.1126/sciadv.adk6911

Springer Link. (2017). *Cryo-EM structure determination in neurodegeneration*. Retrieved from https://link.springer.com/article/10.1007/s00401-017-1707-9

World Health Organization. (n.d.). *Dementia*. Retrieved from https://www.who.int/news-room/fact-sheets/detail/dementia

Royal Society of Chemistry. (2022). *Advances in cryo-EM and amyloid detection*. Retrieved from https://pubs.rsc.org/en/content/articlelanding/2022/FD/D2FD00034B